

The ROSAT Brightest Cluster Sample (BCS): The cluster X-ray luminosity function within $z = 0.3$

H. Ebeling¹, A.C. Edge, A.C. Fabian, S.W. Allen, C.S. Crawford
Institute of Astronomy, Madingley Road, Cambridge CB3 0HA, UK

and

H. Böhringer
MPI für extraterrestrische Physik, Giessenbachstr., D-85740 Garching, Germany

ABSTRACT

We present and discuss the X-ray luminosity function (XLF) of the ROSAT Brightest Cluster sample (BCS), an X-ray flux limited sample of clusters of galaxies in the northern hemisphere compiled from ROSAT All-Sky Survey data. The BCS allows the local cluster XLF to be determined with unprecedented accuracy over almost three decades in X-ray luminosity and provides an important reference for searches for cluster evolution at higher redshifts.

We find the significance of evolution in both the XLF amplitude and in the characteristic cluster luminosity L_X^* to be less than 1.8σ within the redshift range covered by our sample thereby disproving previous claims of strong evolution within $z \lesssim 0.2$.

Subject headings: galaxies: clusters: general — cosmology: observations — X-rays: general

1. Introduction

The ROSAT Brightest Cluster sample (BCS, Ebeling et al. 1996b, hereafter Paper I) is a 90% complete, flux limited sample of the 199 X-ray brightest clusters of galaxies in the northern hemisphere ($\delta \geq 0^\circ$), at high Galactic latitudes ($|b| \geq 20^\circ$, with redshifts $z \leq 0.3$, fluxes higher than 4.45×10^{-12} erg cm⁻² s⁻¹ and luminosities higher than 5×10^{42} erg s⁻¹ in

¹also: Institute for Astronomy, 2680 Woodlawn Dr, Honolulu HI 96822, USA; email: ebeling@ifa.hawaii.edu

the 0.1–2.4 keV band. Second in size only to the XBACs sample of Ebeling et al. (1996a), the BCS is one of the largest statistical cluster samples compiled at X-ray wavelengths to date. It is the only large-scale sample available today that is not only X-ray *flux limited* but also X-ray *selected* in the sense that the BCS, unlike the XBACs, is not limited to systems initially found in optical surveys but contains clusters selected by their X-ray properties only.

The BCS thus represents an ideal sample for studies of the formation, distribution and evolution of structure on the largest metric and mass scales. Providing important constraints on the cosmological parameters governing cluster evolution, the X-ray luminosity function (XLF) of clusters of galaxies represents a particularly vital statistic in this context.

Several previous studies based on much smaller samples of typically 50 clusters found the evolution in the cluster X-ray luminosity function to be ‘negative’ in the sense that X-ray luminous clusters are more numerous now than they were in the past (Edge et al. 1990; Gioia et al. 1990; Henry et al. 1992; David et al. 1993). They were, however, not only in conflict with other studies, which found no evidence for cluster evolution (e.g., Kowalski et al. 1984), but also somewhat inconsistent among themselves. The strong evolution seen by Edge et al. (1990) in their sample of 46 X-ray bright clusters at high Galactic latitude and $z \leq 0.18$ is not present in the first two redshift bins (44 clusters at $0.14 \leq z \leq 0.3$) of the sample of Gioia et al. (1990) and Henry et al. (1992) who find significant evolution only at $z > 0.3$. More recently, two studies found no sign of evolution at all in the XLF of samples of Abell and ACO clusters at $z \leq 0.36$ (Briel & Henry 1993) and $z \leq 0.15$ (Burg et al. 1994), respectively. However, these samples were neither X-ray selected nor X-ray flux limited and may thus not be fair representations of the cluster population in general. At considerably higher redshifts ($z > 0.5$) on the other hand, studies based on yet smaller samples observed in deep X-ray pointings (Bower et al. 1994; Castander et al. 1994; Castander et al. 1995) suggest a significant drop in the cluster space density as compared to the value observed locally.

Although the overall evidence is thus in favor of negative evolution of the cluster XLF at least for X-ray luminous clusters at redshifts well in excess of 0.3, the overall picture is anything but clear. With the completion of the BCS we are now able to provide a definitive answer to the question of whether cluster evolution is significant at low to intermediate redshifts and, in any case, provide an accurate determination of the local cluster XLF as a much-needed reference for ongoing and future evolutionary studies at higher redshifts. The implications of our findings for cosmological models of cluster evolution will be addressed in a forthcoming paper (Ebeling et al., in preparation). We assume $H_0 = 50 \text{ km s}^{-1} \text{ Mpc}^{-1}$ and $q_0 = 0.5$ throughout this paper.

2. The BCS XLF and its parametrization

The BCS as published in Paper I is only 90% complete and corrections for incompleteness need to be applied to account for clusters missing from the sample. In doing this we use a selection function based on the z, L_X distribution of the serendipitous detections in our sample (see §7.1 of Paper I).

We use the usual definition of the unbinned, differential XLF for a sample with flux limit $f_{X,\text{lim}}$:

$$\text{XLF}(L_X, z, f_{X,\text{lim}}) = \frac{dn(L_X, z, f_{X,\text{lim}})}{dL_X}$$

where $dn(L_X, z, f_{X,\text{lim}})$ is the space density of clusters with X-ray fluxes above the flux limit and X-ray luminosities within an interval dL_X around L_X . Since we use an unbinned representation, dn is given for each cluster by $1/V(L_X, z, f_{X,\text{lim}})$, i.e., the inverse search volume defined by the luminosity distance at which the X-ray flux from a cluster with intrinsic luminosity L_X would equal the flux limit of the sample. The systems' X-ray temperatures as listed in Paper I are used in the computation of K corrections.

We use a Schechter function (Schechter 1976) of the form

$$\frac{dn}{dL_X}(L_X) = A \exp(-L_X/L_X^*) L_X^{-\alpha}$$

to model the XLF and determine A , L_X^* and α in a maximum-likelihood fit to the unbinned data.

Table 1 gives an overview of the fit results obtained in all five standard energy bands currently in use within the scientific community: 0.1 – 2.4, 0.5 – 2.0, 0.3 – 3.5, and 2 – 10 keV, as well as the pseudo-bolometric band from 0.01 to 100 keV. We discuss the results in detail in the following paragraphs.

Figure 1 shows the differential XLF for the BCS in the generic 0.1 – 2.4 keV band of the ROSAT observatory. We test the robustness of the fit by comparing it to the XLF obtained for the larger, 80% complete BCS (unpublished, cf. Paper I) and find excellent agreement. Also shown in Figure 1 are the XLF data points for the high-galactic-latitude sample of Edge et al. (1990, hereafter B50) (open diamonds) which is X-ray flux limited in the 2 – 10 keV band. Since all 46 B50 clusters have measured X-ray temperatures, the conversion of their luminosities to the 0.1 – 2.4 keV band of the BCS is less inaccurate than the opposite operation, i.e., the conversion of the BCS luminosities into the 2 – 10 keV band, which relies heavily on temperature estimates rather than measured values. To assess the impact of band conversion effects we make the comparison between the XLFs of the B50 and the BCS in either band. In the 0.1 – 2.4 keV band we find the XLF for the B50 to

be, in general, in good agreement with the BCS XLF. At low X-ray luminosities, however, the best Schechter function fit for the B50 (the dotted line in Figure 1 and obtained with the same ML algorithm used throughout for the fitting of the BCS XLFs) severely underpredicts the observed volume density of clusters, indicating incompleteness of the B50 at $L_X \lesssim 1 \times 10^{44} \text{ erg s}^{-1}$ (0.1 – 2.4 keV). This is, however, not surprising given that the B50 is, by design, only flux-limited in the 2 – 10 keV band.

Figure 2 shows the BCS XLF in the ROSAT hard band covering the energy range from 0.5 to 2.0 keV. Note that, like for all other energy bands discussed in the following, the conversion from the original BCS band (0.1 – 2.4 keV) to the ROSAT hard band was performed for each cluster individually using the X-ray temperatures and Galactic column densities given in Table 2 of Paper I and assuming a metallicity of 0.3 of the solar value. Also shown in Figure 2 are the data of the XLF of groups and poor clusters of galaxies as presented by Burns et al. (1996, hereafter BLL) and their best power-law XLF. Note the good agreement between the two samples as well as the respective XLF models in the overlap region between $3 \times 10^{42} \text{ erg s}^{-1}$ (the lowest luminosity of any BCS cluster) and $2.6 \times 10^{43} \text{ erg s}^{-1}$ (the highest luminosity of BLL’s poor cluster sample)². Finally, we overlay in Fig. 2 the best fitting Schechter function XLF determined by De Grandi (1996) for the 111 clusters of the BSGC-KP sample, a subset of a larger ROSAT cluster sample under compilation in the southern hemisphere (Guzzo et al. 1995). For luminosities in excess of $\sim 2 \times 10^{43} \text{ erg s}^{-1}$ De Grandi’s XLF is in very good agreement with the best-fitting BCS Schechter function. Below this value the BSGC-KP XLF falls increasingly below both the BLL and the BCS fits, reaching a deviation of a factor of 2 and 3, respectively, at the lower end of the BSGC-KP luminosity range.

The reference in the 0.3 – 3.5 keV band is the EMSS cluster sample of Henry et al. (1992). Figure 3 shows the BCS XLF in the 0.3 – 3.5 keV band with the EMSS data points from the first two redshift shells ($0.14 \leq z < 0.2$ and $0.2 \leq z < 0.3$) overlaid as shaded diamonds. (We remind the reader that the power law descriptions of the EMSS XLF found by Henry and coworkers in these shells are consistent with one another within the errors, so that the comparison with the whole of the BCS made in Figure 3 is legitimate.) Note the very good agreement between the EMSS and BCS luminosity functions, but also the much higher accuracy provided by the BCS. Also shown in Figure 3 is the XLF from the third EMSS redshift shell ($0.3 \leq z < 0.6$). Contrary to our findings for the EMSS XLF for

²We have tested the compatibility of the two samples by comparing the luminosities of the four clusters contained in both the BCS and the BLL sample. We find agreement to within 5% between the respective luminosities for all but one cluster (MKW8) for which the BLL luminosity falls short of the BCS value by 40%.

clusters at $0.14 \leq z < 0.3$, the EMSS XLF of these high-redshift systems differs noticeably from the BCS XLF as the local reference. A detailed re-assessment of the significance of the evolution implied by this discrepancy is presented by Ebeling et al. (in preparation).

Although, in Table 1, we do list the results of a Schechter function fit to the BCS data in the 2 – 10 keV band, the BCS XLF in this hard energy band should be regarded with caution. The 2 – 10 keV band has hardly any overlap with the 0.1 – 2.4 keV BCS detection band, which renders a flux conversion that is largely based on estimated temperatures a dangerous enterprise. Keeping this caveat in mind we nonetheless find the power law description from Piccinotti et al. (1982) to be in good agreement with the BCS XLF irrespective of whether the Virgo cluster is included or not (Figure 4).

The best fit parameters from the Schechter function fit to the B50 data published by Edge et al. (1990), on the other hand, provide an unacceptable fit to the BCS XLF at luminosities in excess of about 1×10^{45} erg s⁻¹, where the fit given by Edge et al. falls significantly below the BCS data. This failure of the original B50 Schechter function fit to describe the BCS XLF is due to an error in the volume calculation in the work of Edge and coworkers. Fitting the B50 data with our maximum likelihood algorithm we find $A = 1.59_{-0.33}^{+0.38} \times 10^{-7}$ Mpc⁻³ (10⁴⁴ erg s⁻¹) ^{$\alpha-1$} , $L_X^* = 8.46_{-1.83}^{+2.69} \times 10^{44}$ erg s⁻¹, and $\alpha = 1.25_{-0.20}^{+0.19}$, in good agreement with the results for the BCS (see Figure 4 and Table 1).

3. Evidence of evolution in the BCS XLF

We search for evidence of evolution by splitting the BCS at a redshift z_{sep} and independently fitting Schechter functions to the data in the two redshift shells thus created. Care has to be taken not to naïvely misinterpret every statistically significant difference between the best fit parameters in the two shells as signature of evolution. In order to avoid effects due to large scale structure, we vary z_{sep} from 0.05 to 0.2 and look for trends that are robust over a range of z_{sep} values. Since, due to the flux-limited nature of our sample, the low-luminosity end of the XLF, and thus α , is ill-constrained for the high-redshift subsample once z_{sep} exceeds $z \sim 0.1$, we fix the power law slope α at its overall best-fit value of 1.85 in the maximum-likelihood fits to the data of either subsample. With α frozen we are thus left with two free parameters, the normalization A and the characteristic luminosity L_X^* .

Figure 5 shows the contours of the C statistic (which is χ^2 distributed) of A and L_X^* for some of these low-redshift and high-redshift subsamples of the BCS as a function of z_{sep} . While differences found at $z_{\text{sep}} \lesssim 0.1$ can be attributed entirely to large-scale structure, a significant decrease in A or L_X^* at higher values of z_{sep} would be indicative of negative

evolution. As, for $0.05 \leq z_{\text{sep}} \leq 0.2$, the 68% confidence contours of the low-redshift and high-redshift subsamples overlap, we conclude that there is no significant evolution in either the amplitude A of the cluster XLF or the characteristic luminosity L_X^* for values of z_{sep} up to 0.2. Since, in the high-redshift subsamples with $z_{\text{sep}} \gtrsim 0.16$, A becomes ill-constrained and increasingly strongly correlated with L_X^* , we also tested for evolution only in L_X^* by holding A constant at its overall best-fit value of $4.33 \times 10^{-7} \text{ Mpc}^{-3} (10^{44} \text{ erg s}^{-1})^{\alpha-1}$, a value well within the 68% confidence contours of all fits shown in Fig. 5. We find the variations in L_X^* to be smaller than 30(37)% for $0.1 < z_{\text{sep}} \leq 0.20(0.22)$ which is less than $1.6(1.8)\sigma$ significant, confirming the no-evolution result of Fig. 5.

As an independent check, we also looked for variations in V/V_{max} as a function of both z and L_X — and found none. A Kolmogorov-Smirnov test finds the distribution of V/V_{max} values (whose median is 0.47) to be consistent with uniformity at the greater than 74% confidence level suggesting again that the cluster space density of the BCS is homogeneous out to the limiting redshift of $z = 0.3$.

4. Conclusions

Using the ROSAT Brightest Cluster Sample (BCS) as presented by Ebeling et al. (1996b) we have established the local X-ray luminosity function (XLF) of clusters of galaxies within $z = 0.3$ with unprecedented accuracy. We find the XLF to be well described by a Schechter function whose free parameters A , L_X^* , and α we determine in a maximum-likelihood fit for all X-ray energy bands currently used within the community. Comparing our results with previous measurements of the cluster XLF we find very good agreement with the work of Piccinotti et al. (1982), Henry et al. (1992), and Burns et al. (1996), as well as with the XLF for the B50 sample of Edge et al. (1990) when the same maximum likelihood algorithm is used to determine the best Schechter function fit.

We find no significant variations in the amplitude or the characteristic luminosity of the best-fitting Schechter function as a function of redshift. Also, the distribution of V/V_{max} values is consistent at the 74% confidence level with a non-evolving space density of clusters out to $z = 0.3$. Our findings do thus not confirm the claim of strong evolution at $z \lesssim 0.2$ made by Edge and coworkers but support the notion of Ebeling et al. (1995) that the apparent signature of evolution in the B50 sample is due to a combination of its high X-ray flux limit in the 2 – 10 keV band and a pronounced, if statistically insignificant, dearth of very X-ray luminous clusters around a redshift of about 0.15.

H.E. thanks Pat Henry for helpful discussions about maximum-likelihood fitting and

cluster evolution. H.E. acknowledges financial support from a European Union EARA Fellowship and SAO contract SV4-64008. A.C.E., A.C.F. and S.W.A. thank the Royal Society for support. C.S.C. acknowledges financial support from a PPARC Advanced Fellowship. H.B. thanks the BMFT for financial support through the Verbundforschung programme.

REFERENCES

- Bower, R.G., Böhringer, H., Briel, U.G., Ellis, R.S., Castander, F.J., Couch, W.J. 1994, MNRAS, 268, 345
- Briel, U.G. and Henry, J.P. 1993, A&A, 278, 379
- Burg, R., Giacconi, R., Forman, W., Jones, C. 1994, ApJ, 422, 37
- Burns, J.O., Ledlow, M.J., Loken, C., Klypin, A., Voges, W., Bryan, G.L., Norman, M.L., White, R.A. 1996, ApJ, 467, L49 (BLL)
- Castander, F.J., Ellis, R.S., Frenk, C.S., Dressler, A., Gunn, J.E. 1994, ApJ, 424, L79
- Castander, F.J., Bower, R.G., Ellis, R.S., Aragon-Salamanca, A., Mason, K.O., Hasinger, G., McMahon, R.G., Carrera, F.J., Mittaz, J.P.D., Perez-Fournon, I., Lehto, H.J. 1995, Nature, 377, 39
- David, L.P., Slyz, A., Jones, C., Forman, W., Vrtilik, S.D., Arnaud, K.A. 1993, ApJ, 412, 479
- De Grandi, S. 1996, in MPE Report 263, Proceedings of Röntgenstrahlung from the Universe, ed. Zimmermann H.U., Trümper J., Yorke H. (Munich: MPE), 577
- Ebeling, H., Böhringer, H., Briel, U.G., Voges, W., Edge, A.C., Fabian, A.C., Allen, S.W. 1995, in Wide Field Spectroscopy and the Distant Universe, ed. S.J. Maddox & A. Aragón-Salamanca, (Singapore: World Scientific), 221
- Ebeling, H., Voges, W., Böhringer, H., Edge, A.C., Huchra, J.P., Briel, U.G. 1996a, MNRAS, 281, 799
- Ebeling, H., Edge, A.C., Böhringer, H., Allen, S.W., Crawford, C.S., Fabian, A.C., Voges, W., Huchra, J.P. 1996b, MNRAS, submitted (Paper I)
- Edge, A.C., Stewart, G.C., Fabian, A.C., Arnaud, K.A. 1990, MNRAS, 245, 559
- Gioia, I.M., Henry, J.P., Maccacaro, T., Morris, S.L., Stocke, J.T., Wolter, A. 1990, ApJ, 356, L35
- Guzzo, L. et al. 1995, in Wide Field Spectroscopy and the Distant Universe, ed. S.J. Maddox & A. Aragón-Salamanca, (Singapore: World Scientific), 205
- Henry, J.P., Gioia, I.M., Maccacaro, T., Morris, S.L., Stocke, J.T., Wolter, A. 1992, ApJ, 386, 408
- Kowalski, M.P., Ulmer, M.P., Cruddace, R.G., Wood, K.S. 1984, ApJS, 56, 403
- Piccinotti, G., Mushotzky, R.F., Boldt, E.A., Holt, S.S., Marshall, F.E., Serlemitsos, P.J., Shafer, R.A. 1982, ApJ, 253, 485

Schechter, P. 1976, ApJ, 203, 297

Table 1. Best fit values of the Schechter function parameters A , L_X^* , and α

Energy Band	A^\dagger	$L_X^{*\ddagger}$	α
0.1–2.4 keV	$5.06^{+0.50}_{-0.46}$	$9.10^{+2.06}_{-1.49}$	$1.85^{+0.09}_{-0.09}$
0.5–2.0 keV	$3.32^{+0.36}_{-0.33}$	$5.70^{+1.29}_{-0.93}$	$1.85^{+0.09}_{-0.09}$
0.3–3.5 keV	$4.95^{+0.48}_{-0.45}$	$10.7^{+2.4}_{-1.8}$	$1.82^{+0.08}_{-0.09}$
2–10 keV	$2.35^{+0.22}_{-0.18}$	$12.6^{+2.2}_{-1.8}$	$1.54^{+0.05}_{-0.06}$
bolometric	$6.41^{+0.70}_{-0.61}$	$37.2^{+16.4}_{-3.8}$	$1.84^{+0.09}_{-0.04}$

† in units of $10^{-7} \text{ Mpc}^{-3} (10^{44} \text{ erg s}^{-1})^{\alpha-1}$

‡ in units of $10^{44} \text{ erg s}^{-1}$

Errors given correspond to 68% confidence for one interesting parameter ($\Delta C = 1$).

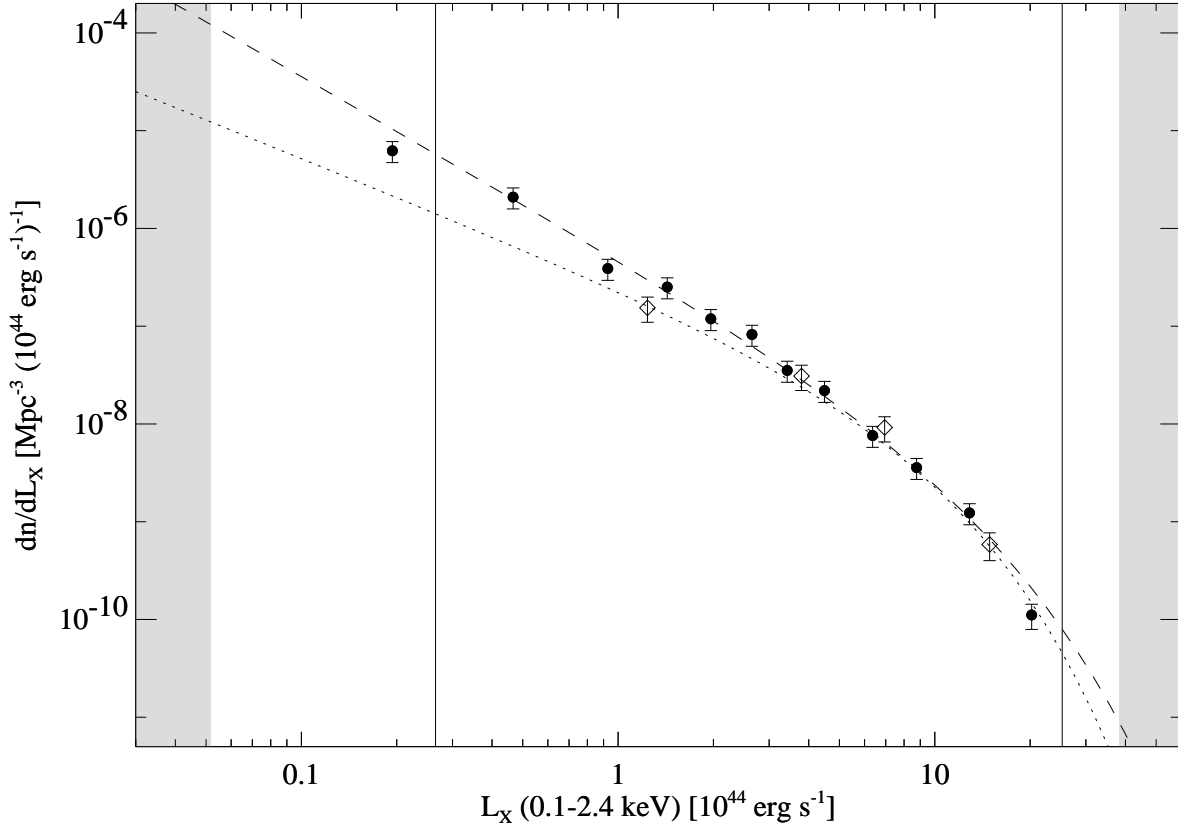


Fig. 1.— The X-ray luminosity function (filled circles) for the ROSAT Brightest Cluster Sample in the 0.1 – 2.4 keV band. The data are grouped such that each bin contains 17 clusters, except the highest-luminosity one which contains 12 clusters. The dashed line shows the best Schechter function fit. The shaded region marks the luminosity range not covered by the BCS. Overlaid is the XLF of the B50 sample of Edge et al. (1990) when converted to the 0.1 – 2.4 keV band and grouped such that each bin contains 12 clusters, except the highest-luminosity one which contains 10 clusters (open diamonds). The luminosity range covered by the B50 in the 0.1 – 2.4 keV band is indicated by the solid vertical lines; the best Schechter function fit to the unbinned B50 data is represented by the dotted line.

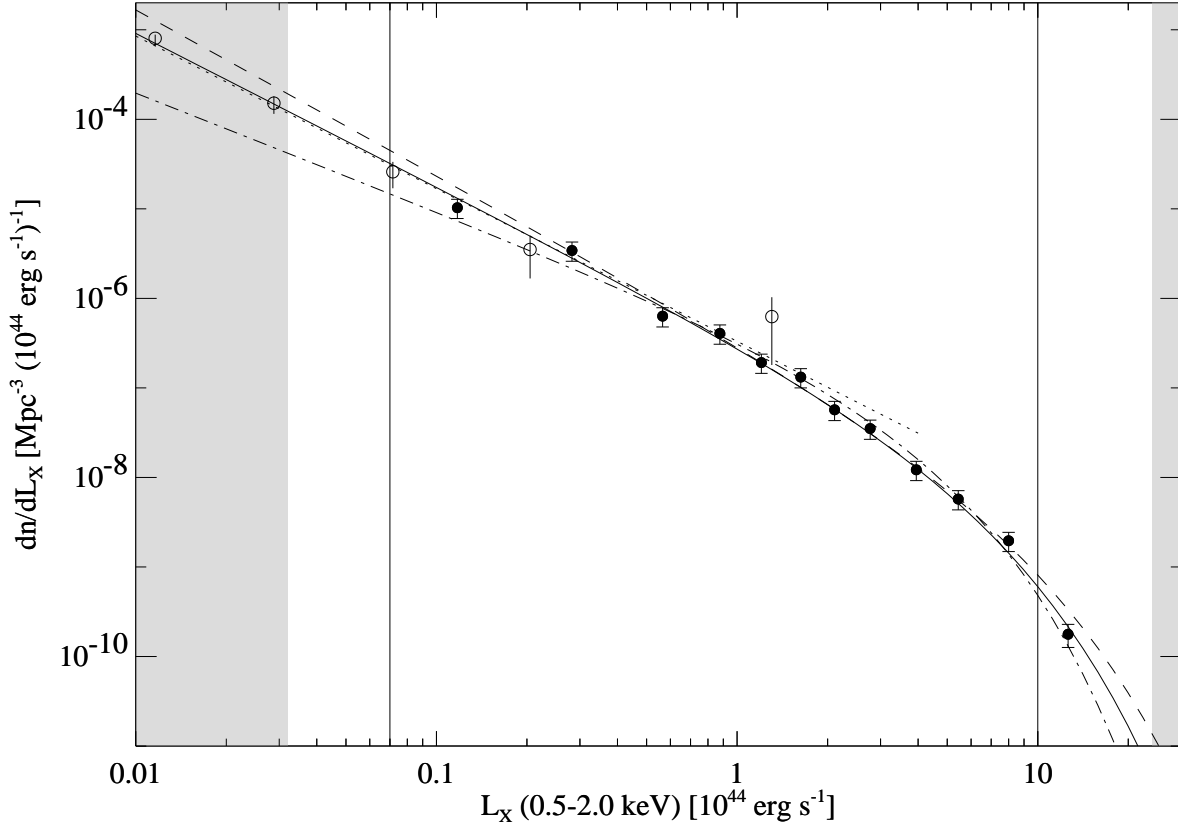


Fig. 2.— The cluster X-ray luminosity function in the 0.5 – 2.0 keV band. The dashed curve represents the best Schechter function fit to the BCS data (filled circles; binning as in Figure 1). The open circles and the dotted line show the group XLF and the corresponding best-fitting power law from BLL. The solid line represents the best Schechter function fit to the XLF obtained by combining the binned BCS data with the first 4 data points of the groups XLF as determined by BLL. The dot-dashed line, finally, shows the XLF determined by De Grandi (1996) for a sample of 111 clusters selected from ROSAT data in the southern hemisphere. The luminosity range of this sample is indicated by the solid vertical lines (De Grandi, private communication).

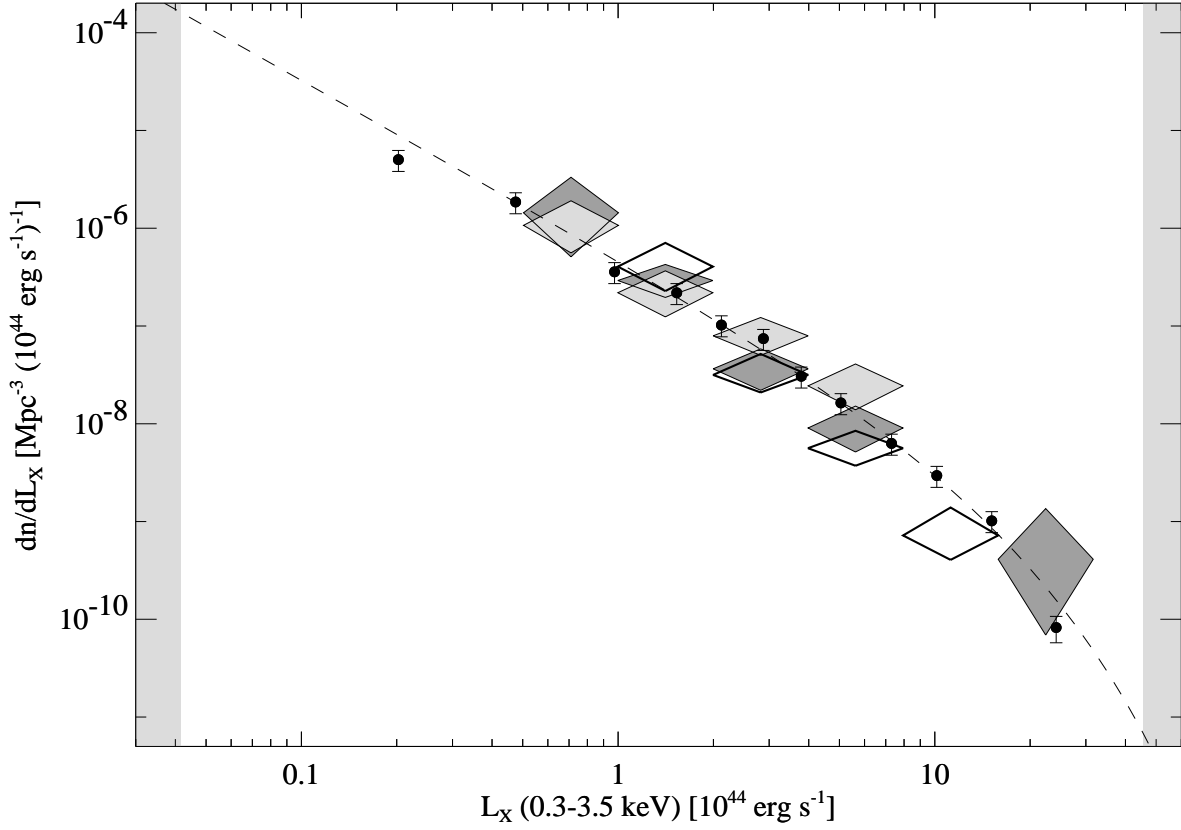


Fig. 3.— The cluster X-ray luminosity function in the 0.3 – 3.5 keV band. The dashed curve represents the best Schechter function fit to the BCS data (filled circles; binning as in Figure 1). The diamonds in light and dark shading show the EMSS XLF of Henry et al. (1992) in the $0.14 \leq z < 0.2$ and the $0.2 \leq z < 0.3$ redshift shell, respectively, while the EMSS XLF in the $0.3 \leq z < 0.6$ shell is represented by open diamonds.

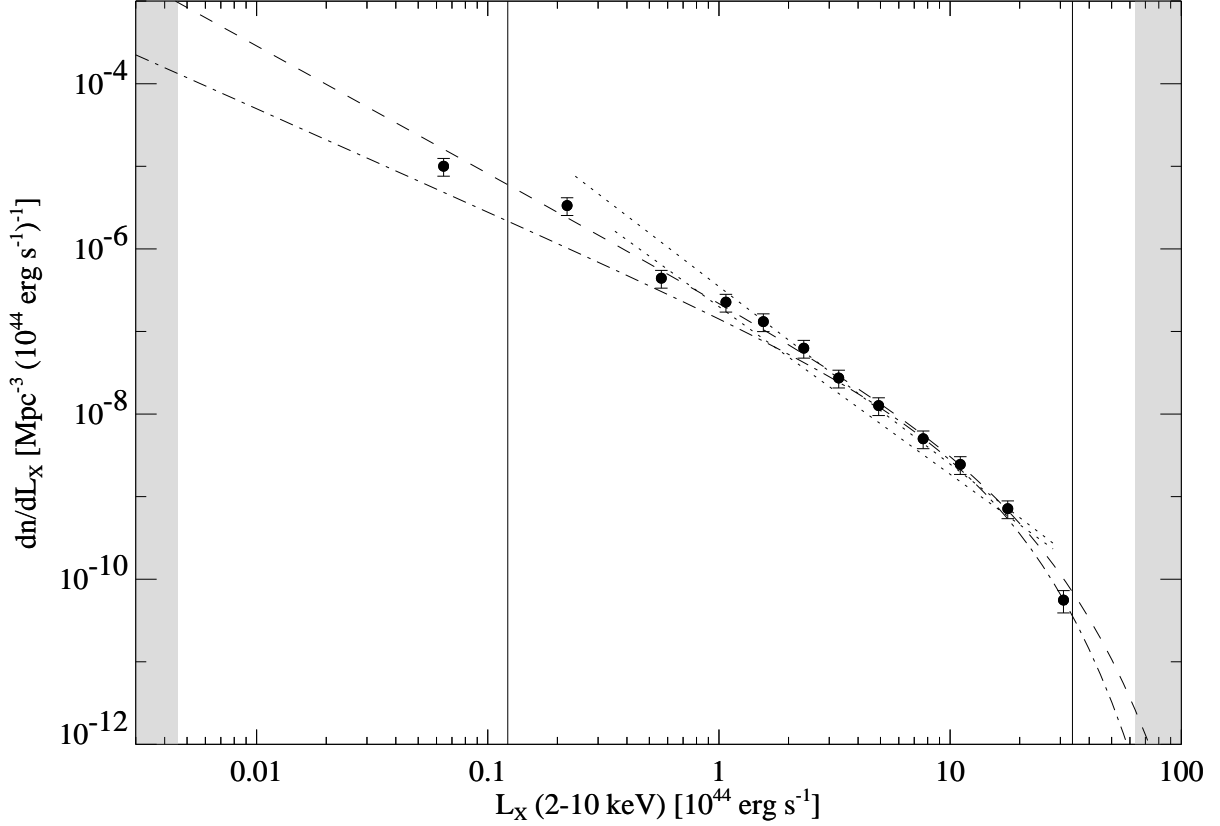


Fig. 4.— The cluster X-ray luminosity function in the 2 – 10 keV band. The dashed curve represents the best Schechter function fit to the BCS data (filled circles; binning as in Figure 1). The two dotted lines show the power-law representations of the XLF of Piccinotti et al. (1982) with and without the Virgo cluster, respectively. The dot-dashed line, finally, represents our best Schechter function fit to the B50 data of Edge et al. (1990) which covers the luminosity range bounded by the solid vertical lines.

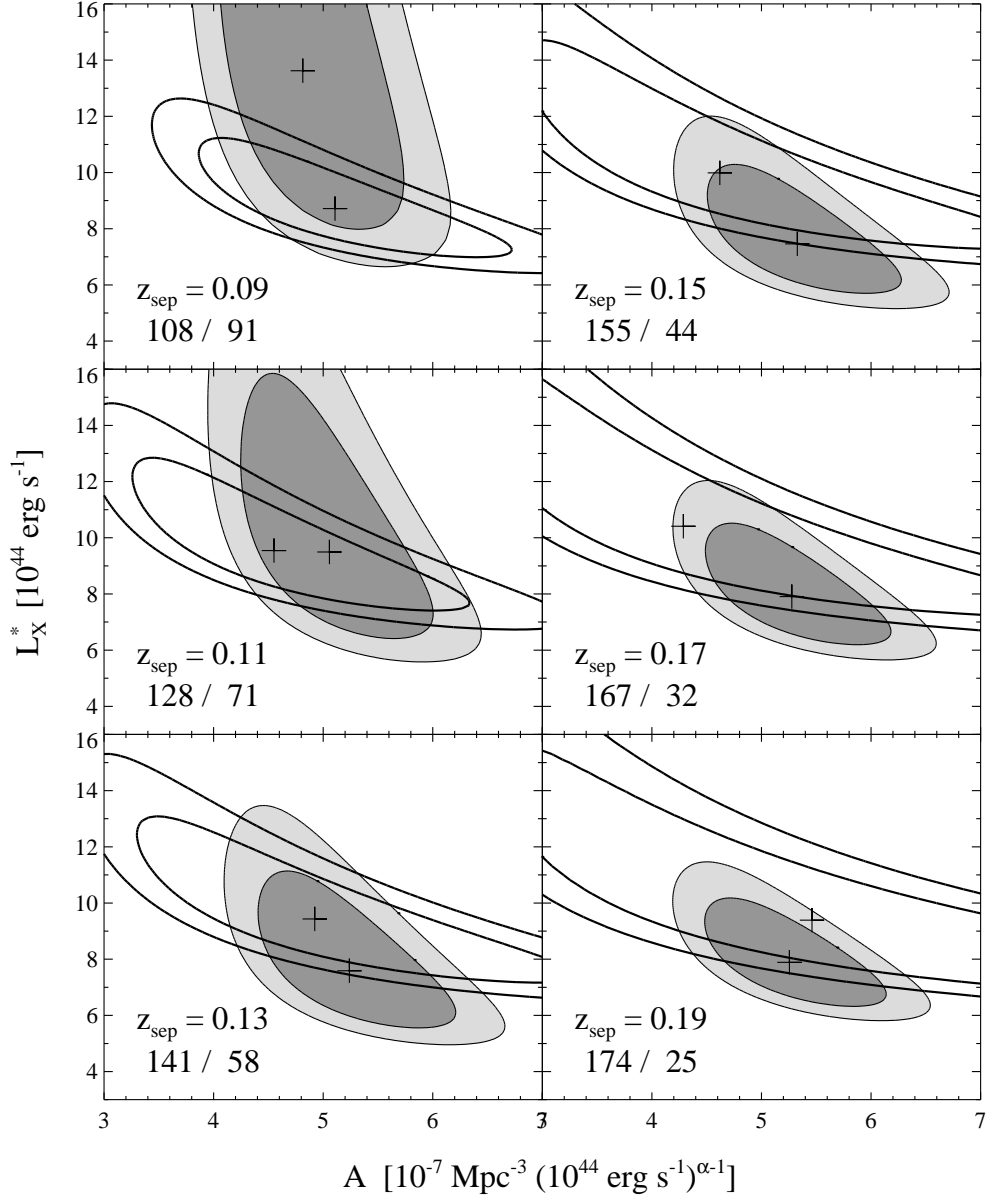


Fig. 5.— Likelihood ratio contours (68 and 90% confidence for two interesting parameters, i.e., $\Delta C = 2.30, 4.61$) in A and L_X^* for BCS subsamples obtained by splitting the sample at an intermediate redshift z_{sep} . The various values of z_{sep} are shown in the lower left corner of each plot as are the numbers of clusters in the low- and the high-redshift subsample, respectively. Filled contours correspond to the low-redshift subsamples; the contours for the high-redshift subsamples are shown as bold solid lines. In the Schechter function fits, α was kept frozen at its global best-fit value of 1.85.